Supporting information for

Label-Free Single-Molecule Thermoscopy Using a Laser-Heated Nanopore

By Hirohito Yamazaki, [†] *Rui Hu,* [†, §] *Robert Y. Henley,* [†] *Justin Halman,* [‡] *Kirill A. Afonin,* [‡] *Dapeng Yu,* [§] *Qing Zhao,* [§] *and Meni Wanunu* [*, †]

[†] Department of Physics, Northeastern University, Boston, Massachusetts 02115

[‡] Department of Chemistry, University of North Carolina at Charlotte, 9201 University City Boulevard, Charlotte, North Carolina 28223, United States

[§] State Key Laboratory for Mesoscopic Physics, School of Physics, Peking University, Beijing 100871, People's Republic of China

Corresponding Author

E-mail: wanunu@neu.edu

Phone: +1-617-373-7412

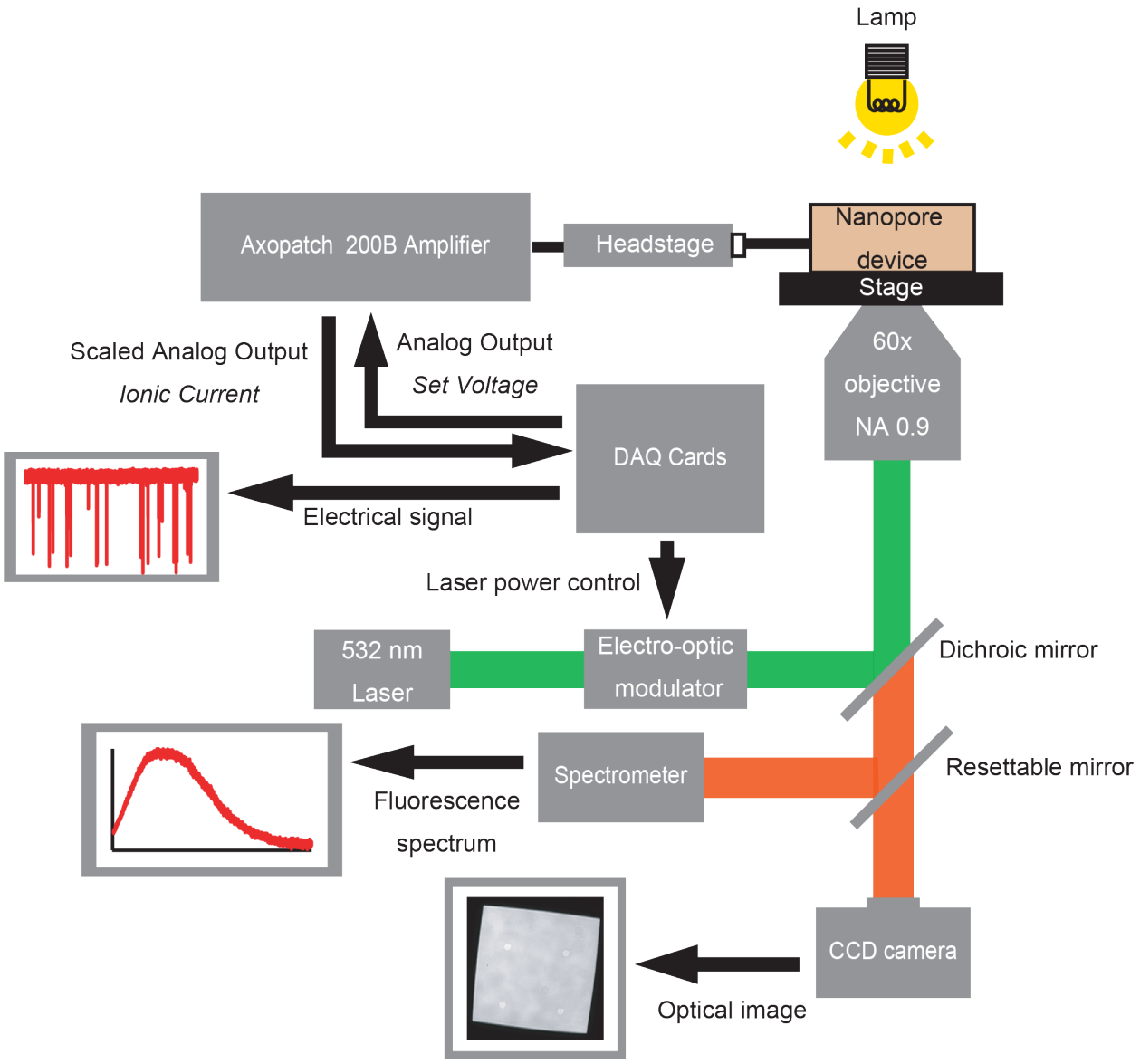

Figure S1. Nanopore device with optical setup. Nanopore device was placed in a Faraday cage. 532 nm laser (Coherent) was focused on a SiN_x membrane using a N.A. 0.9, 60x air objective lens (UPlan APO, Olympus), and an XY automated stage (Applied Scientific Instrumentation) was used to control the laser position. The system was atop an inverted microscope (Olympus IX71) with a manual focus objective turret. Fluorescence spectra and SiN_x chip images were detected using an optical-fiber spectrometer (Thorlabs) and a CCD camera (Aihome), respectively. Laser power was controlled by an electro-optic modulator (Conoptics). An Axopatch 200B patch-clamp amplifier (Molecular Devices) was used for monitoring the electrical current and applying voltage to the nanopore. Two DAQ boards (National Instruments PCI-6230 and PCIe-6351) were used for applying voltage waveforms and digitizing the analog output current signal from the Axopatch, respectively. For thermoscopy, ion current drops, which signaled molecular capture, triggered the output of a voltage ramp to the electro-optic modulator power amplifier (M302, Conoptics), which has a fast time response (4 µs rise time).

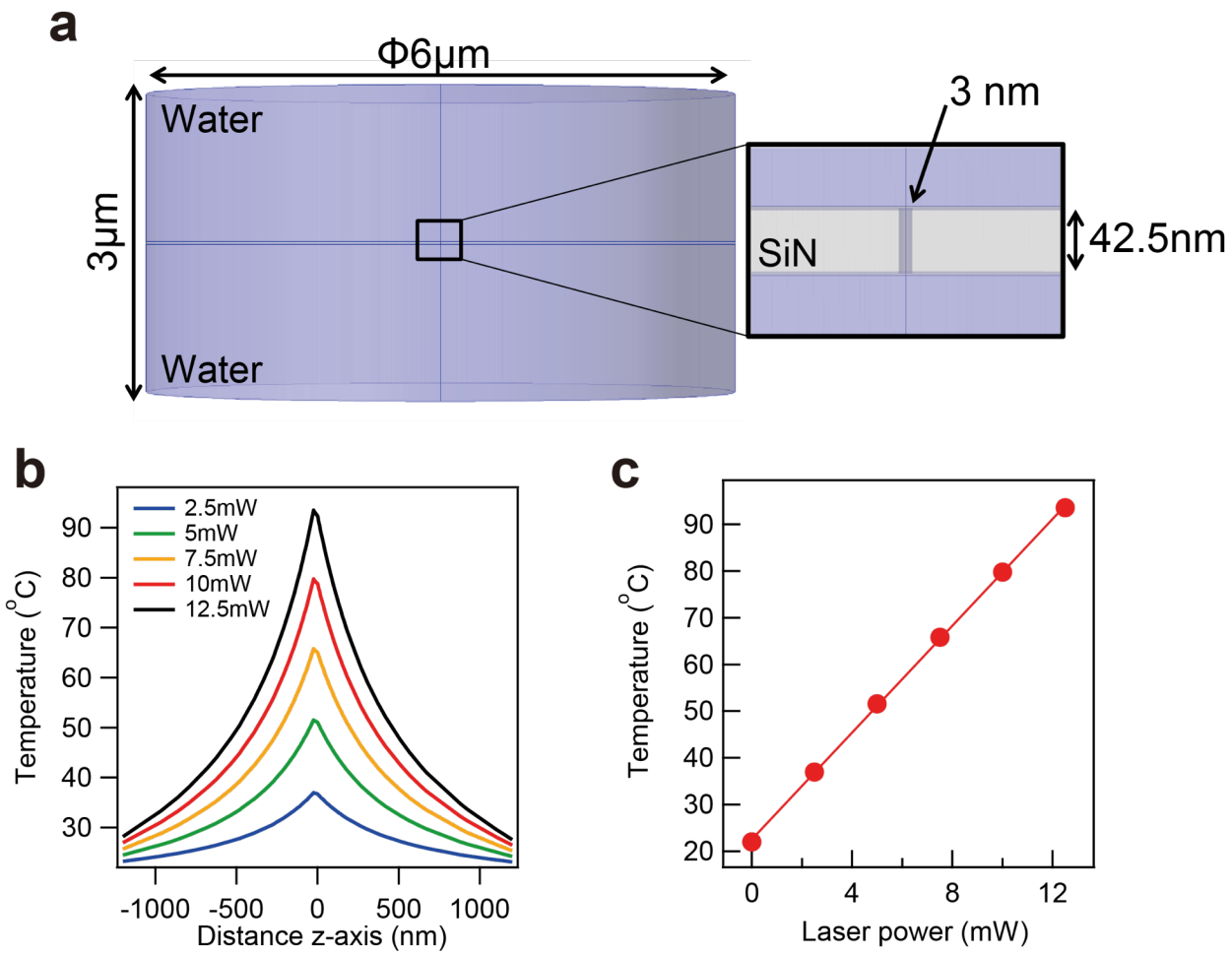

Figure S2. (a) Physical pore model built in COMSOL. (b) Temperature profile along the pore axis for P = 0-12.5 mW. **c**, Peak temperature (T_p) at the pore vs. laser power.

We have used steady-state finite-element simulations to calculate temperature in the nanopore vicinity. The steady-state finite element simulation software we used was COMSOL Multiphysics. Modeling of heat transfer is implemented by applying the first law of thermodynamics (Equation 1):

$$Q = \rho C_p \frac{\partial T}{\partial t} + \nabla \cdot (-k \nabla T) \quad (1)$$

In the equations above, $Q, C_p,\ k$ and T are the heat flux, density, thermal conductivity, specific heat capacity, and temperature, respectively. In COMSOL, we used the heat transfer module which calculates a steady-state solution for coupled heat transfer of fluid and solid. Fig. S2a shows the geometry we used for the simulation. The simulated cylinder had a height and diameter of 3 and 6 μm, respectively. In the middle of the simulation, we placed a 42.5-nm-thick SiN_x membrane that contains a 3-nm diameter pore. This thickness was based on an actual case scenario for the open-pore current and ion-current blockades of dsDNA translocation through a 3-nm diameter pore, as shown in Fig. 3a. The SiN_x membrane was surrounded by water solution. The heat capacity, density and thermal conductivity of SiN_x membrane

were $C_p = 700\ \mathrm{J/(kg \cdot K)}$, k=3 W/(m ·K), and ρ=3100kg/m^3 [1, 2]. For the solution, we chose the properties of water, pre-designed in COMSOL. At the bottom of SiN membrane, we applied the energy flux of a focused laser (P). A Gaussian distribution of intensity was applied on an area with a radius of 360 nm to simulate the focused laser radiation. The energy flux of the focused laser was chosen as $P = I \cdot A \cdot (1-q) \cdot (1-R)$, where $A(\mathrm{absorbance}), q(quantum\ yield)$ and $R(reflection)$were 2.13x10^{-2}, 0.1 and 0.07 and 0.072, respectively. A previous report by Giorgis et. al. has measured the quantum yields of SiN_x films for different Si:N ratios at different temperatures [3]. For amorphous SiN_x, the Si:N ratio can be determined from the refractive index n. We have determined n from ellipsometry to be 2.25, which corresponds to a Si:N ratio of 1.2, and then estimated the quantum of our SiN chip to be 7%. To determine absorbance for our freestanding membranes, we scaled our measured absorbance spectrum for a 200 nm film to the determined membrane thickness of 42.5 nm. Reflection (7.2%) was calculated using $R = (n_1 - n_2)^2/(n_1 + n_2)^2$, where n_1 and n_2 are refractive index of SiN_x (2.25) and water (1.3). Fig. S2b shows the temperature along the pore axis with laser power (z=0 is the pore center). The temperature profile decays rapidly as a function of distance from the membrane, generating a strong thermal gradient. Fig. S2c depicts the peak temperature vs laser power, extracted from the peak temperatures in Fig. S2b.

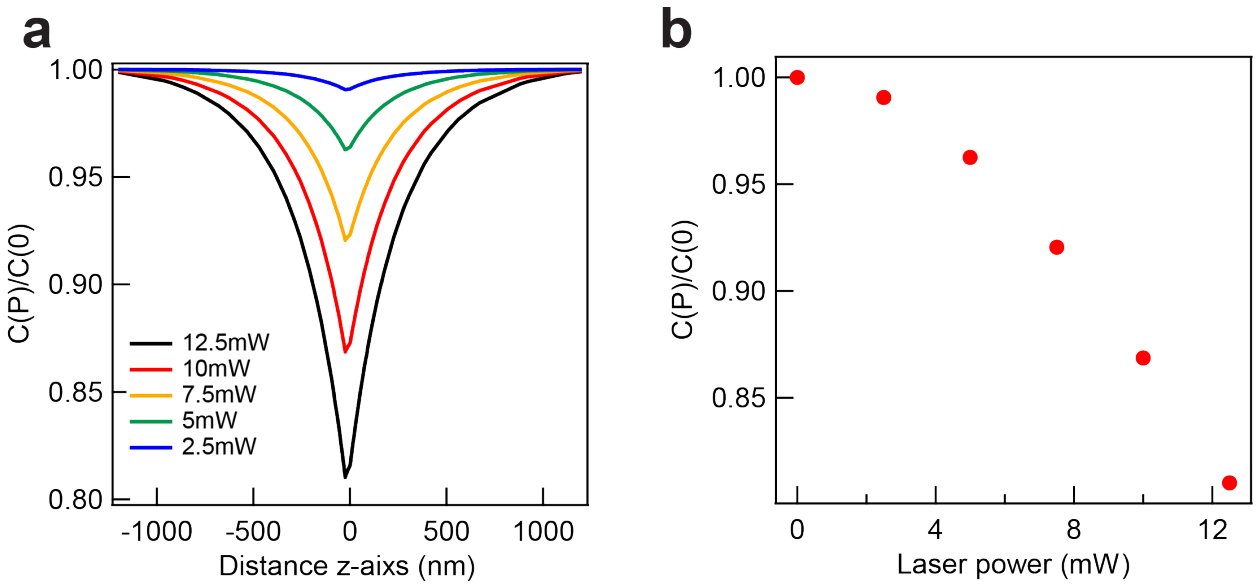

Figure S3. (a) Normalized concentration profile as a function of axial distance from the pore. (b) Mean fractional ion concentration in the pore vs laser power.

From the temperature profile in Figure S2b, we can calculate fractional concentration profile induced by the Soret effect based on eq. 2 and 3. Values of S_T^{∞}, T_0 and T^* were used for KCl based on earlier work, 0.0098 K^{-1}, 193 K, and 297 K, respectively[4]. T_{room} was 295 K. In Figure S3a, we found the concentration inside of nanopore is nearly 20% lower than bulk concentration for the 12.5 mW laser case, and the concentration gradient restores to within 1% of its bulk value ~750 nm away from the pore. Fig. S3b shows fractional ion concentration in the nanopore *vs.* laser power. This fractional concentration exponentially decays as a function of laser power.

The complete form of Eq.3 in the text is

$$I(P)/I(0) = I(T)/I(T_{room}) = C/C_0 \times \frac{A(a+bT)}{A(a+bT_{room})}$$
$$= exp\left[-S_T^{\infty}\left[1-exp\left[\frac{T^*-T}{T_0}\right]\right]\times(T-T_{room})\right]\times\left[\frac{a+b(\Delta T+T_{room})}{a+bT_{room}}\right] \quad (2)$$

which is derived from Equations 1, 2 and 3 in the text.

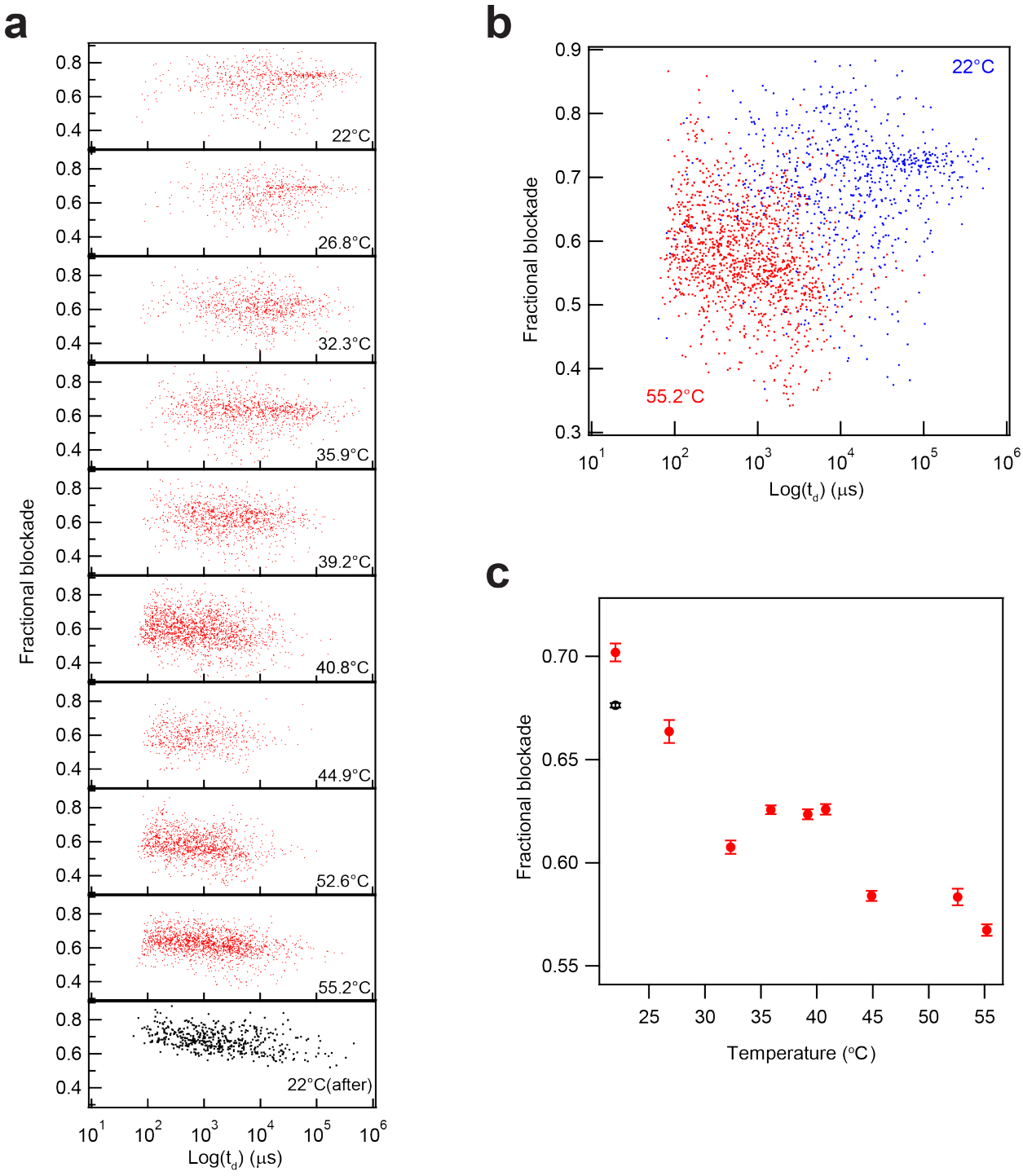

Figure S4. (a) Scatter plots of fractional current blockades vs. Arg-tRNA dwell-time at different temperatures. Black dots show Arg-tRNA translocation after experiment, which shows some hysteresis due to a slight pore expansion. (b) Fractional blockade vs. tRNA dwell time at 22 ^{o}C(blue) and 55.2 ^{o}C(red). (c) Fractional blockade vs. temperature.

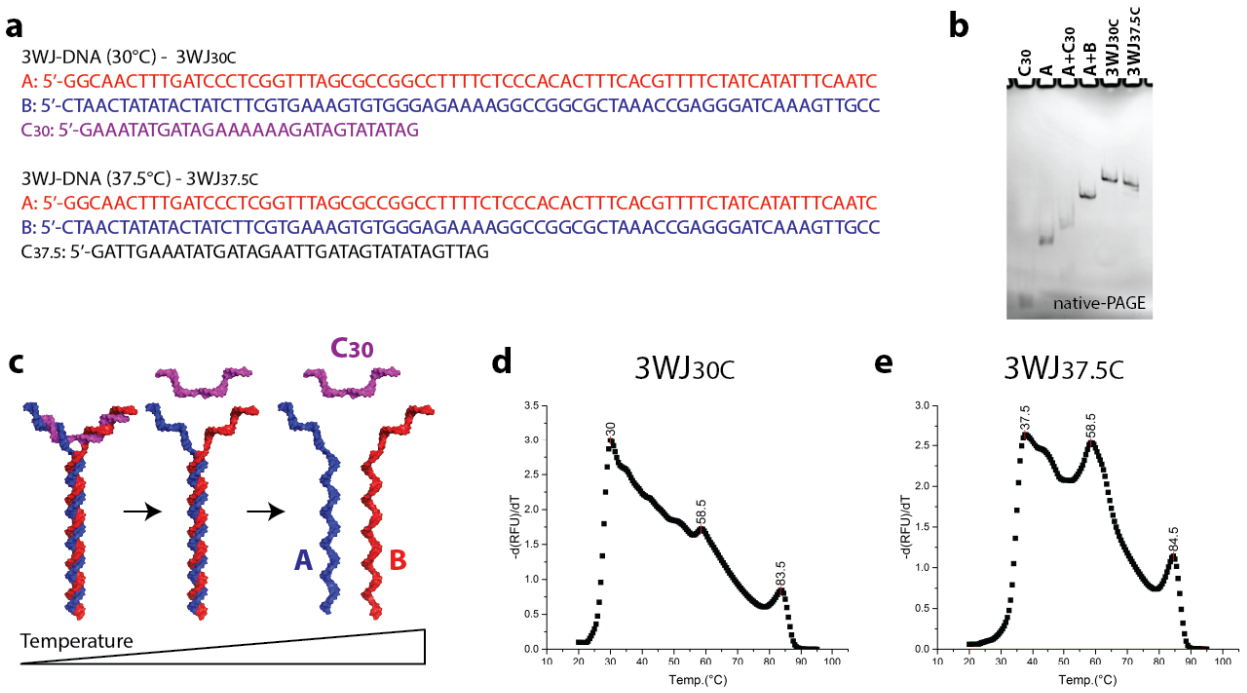

Figure S5. (a) Sequences designed to form 3WJ-DNA nanoparticles with controlled Tm of a branching site. (b) Ethidium Bromide total staining native-PAGE confirms the correct assembly of 3WJ-DNA molecules. (c) 3D model and schematic representation of melting steps for $3WJ_{30C}$ molecule. 3D model was built using Discovery Studio Visualizer(REF). (d)-(e)**,** Melting profiles for 3WJ-DNA molecules, recorded at 260 nm.

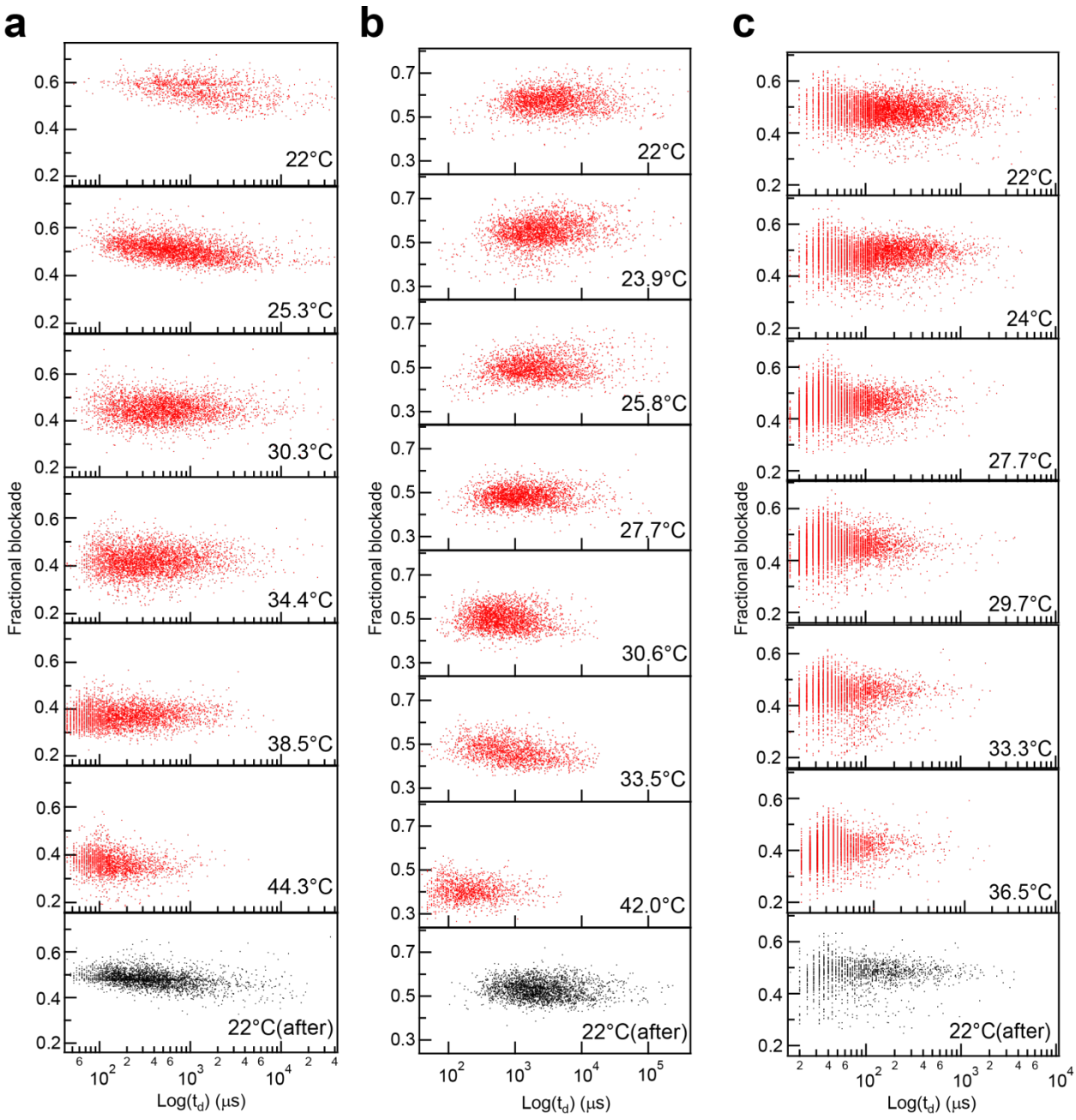

Figure S6. Scatter plots of fractional current blockade vs. dwell time of (a) $3WJ_{37.5}$ (b) $3WJ_{30.0}$ at 150 mV, and (c) $3WJ_{30.0}$ at 300 mV. Scatter plots with black dots were acquired after data at all temperatures was acquired.

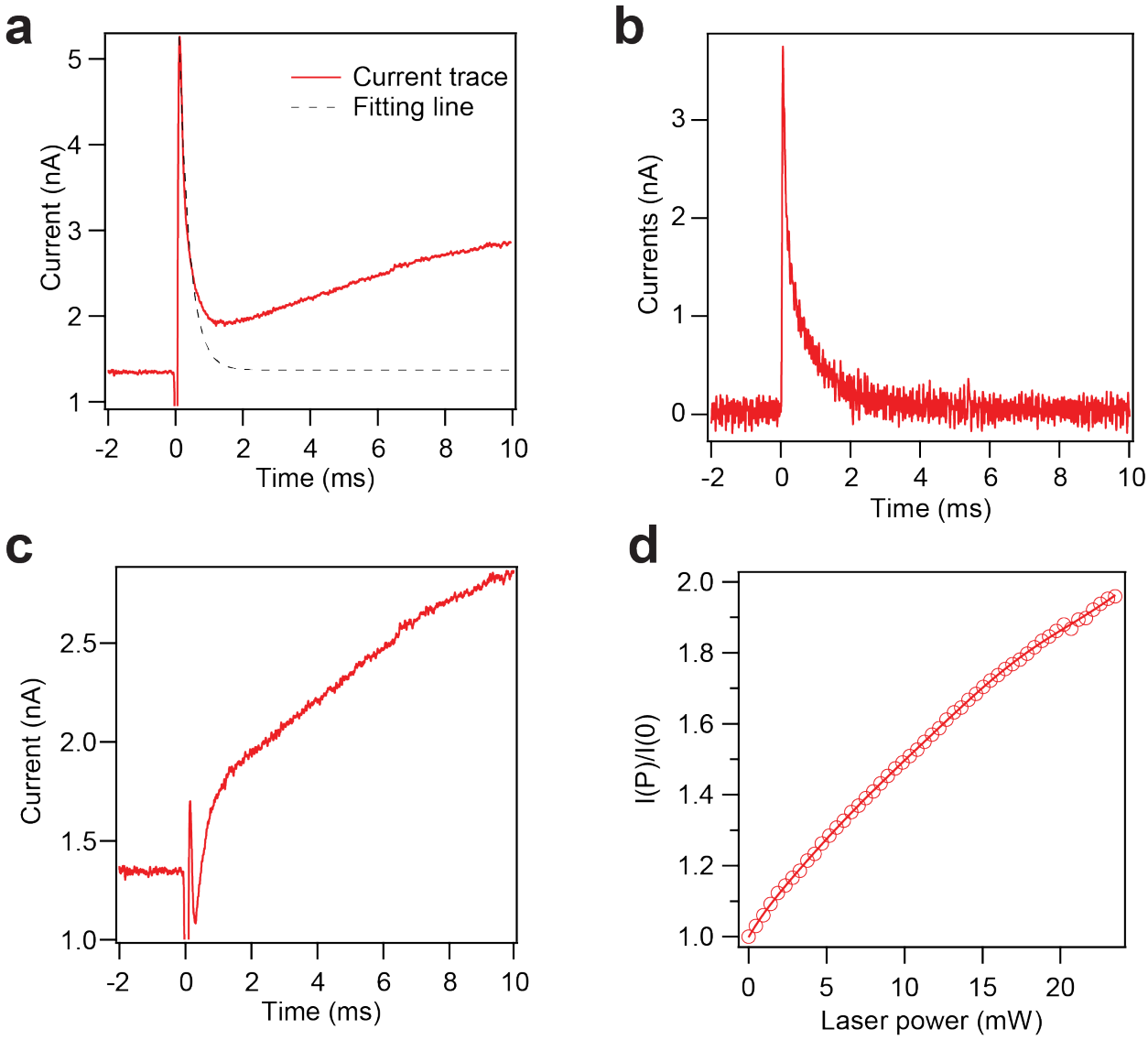

Figure S7. (a) Current trace at the onset of a laser ramp on SiN_x membrane with no pore under application of 300 mV causes a capacitive spike. Black dashed line is exponential fitting to estimate laser induced capacitance change. (b) Current trace during false-triggered laser ramp (no translocations) from the same dataset as the data shown in Figure 5. (c) Current trace subtraction to minimize the capacitive spike effect. (d) I(P)/I(0) vs. laser power for the same pore used in the laser ramp experiment.

When ramping the laser power we observed a capacitive-like spike in the current signal, as shown in Fig. S7a. Since this spike current happens only at the beginning of the ramp, we attribute it to laser-induced membrane capacitance change (Figure S7b). To exclude the spike current, we fit the spike to an

exponential function (see Eq 3 below) and subtract it to obtain a cleaned-up trace as shown in Figure. S7c (~300 µs dead-time at the beginning).

$$I_{spike} = A \cdot \exp(-P/\tau) \quad (3)$$

A and τ were 0.0092 and 0.314 for this experiment. Figure S7d shows I(P)/I(0) vs. Laser power prior to introducing Arg-tRNA for the thermoscopy experiment. The temperature was then calculated based on the I(P)/I(0) data in Figure S7d.

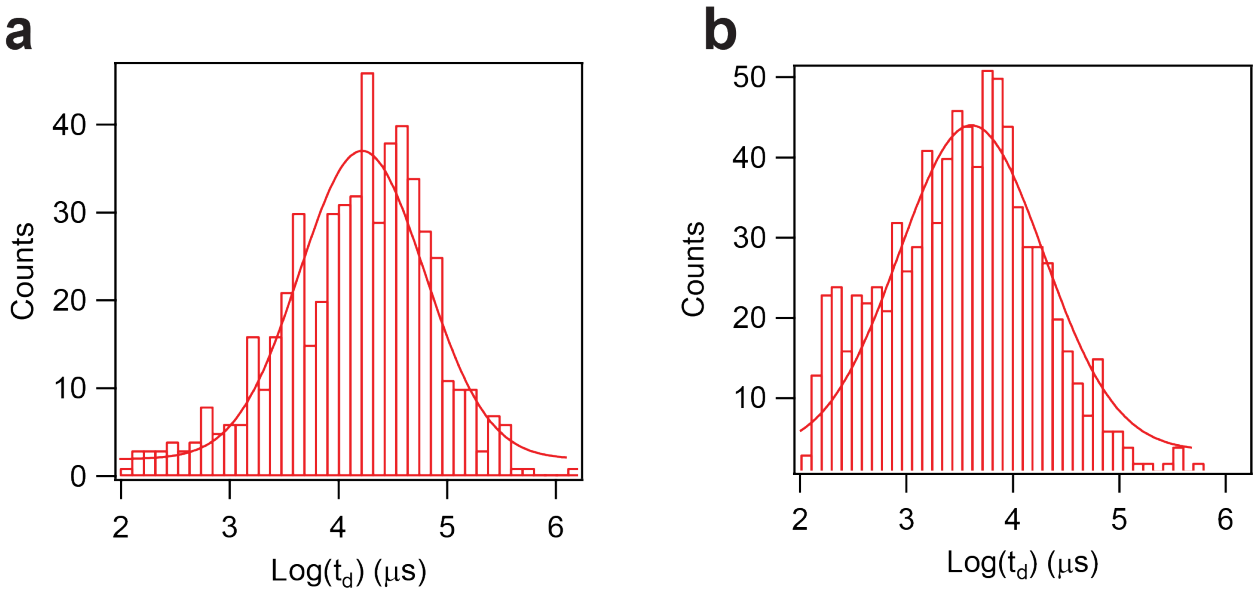

Figure S8. (a) and (b) Arg-tRNA dwell times without laser heating, before and after the single-molecule thermoscopy experiments on the same pore (V = 350 mV). Mean log(t_d) values are 4.21 and 3.62, respectively, the times getting shorter due to a slight pore expansion.

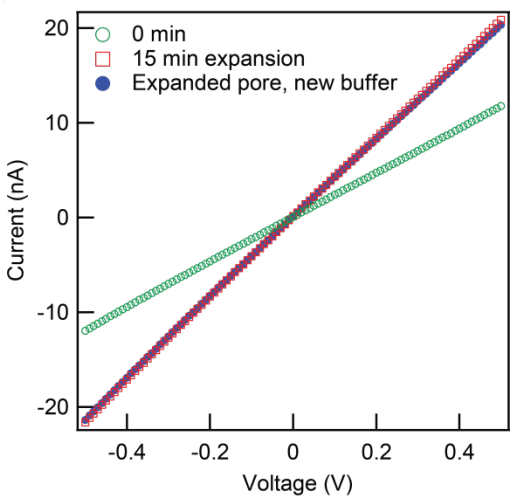

Figure S9. Effect of prolonged laser irradiation on pore size: IV curve of a 5.5 nm SiN pore, before (green) illumination for 15 min with a 42 mW 532 nm focused laser (red squares), and after replenishing the chamber contents with fresh buffer (blue circles), to eliminate the possibility that the increased pore conductance is due to solvent evaporation (all experiments conducted using 0.4 M KCl buffered to pH 7.8).

Supporting References

(1) Ftouni, H.; Blanc, C.; Tainoff, D.; Fefferman, A. D.; Defoort, M.; Lulla, K. J.; Richard, J.; Collin, E.; Bourgeois, O. *Phys. Rev. B* **2015,** 92, 125439.

(2) Alam, M. T.; Manoharan, M. P.; Haque, M. A.; Muratore, C.; Voevodin, A. *J. Micromech. Microeng.* **2012,** 22, 045001.

(3) Giorgis, F.; Vinegoni, C.; Pavesi, L. *Phys. Rev. B* **2000,** 61, 4693-4698.

(4) Römer, F.; Wang, Z.; Wiegand, S.; Bresme, F. *J. Phys. Chem. B* **2013,** 117, 8209-8222.